Journal of Cultural Heritage 58 (2022) 237–244

Contents lists available at ScienceDirect

Journal of Cultural Heritage

journal homepage: www.elsevier.com/locate/culher

Original article

Assessment by laser-induced breakdown spectroscopy of penetration depth in limestones of four nano-biocides based on silver/titanium nanoparticles

Maripaz Mateo[a], Javier Becerra[b], Ana Paula Zaderenko[b], Pilar Ortiz[b], Ginés Nicolás[a,*]

[a] Universidade da Coruña, Campus Industrial de Ferrol, Departamento de Ingeniería Naval e Industrial, Laser Applications Laboratory, C/ Mendizabal s/n, 15403 Ferrol, Spain
[b] Universidad Pablo de Olavide, Departamento de Sistemas Físicos, Químicos y Naturales, Ctra. de Utrera Km.1, ES-41013, Seville, Spain

ARTICLE INFO

Article history:
Received 3 August 2022
Accepted 14 October 2022
Available online 31 October 2022

Keywords:
Biocide
Cultural heritage
LIBS
Depth analysis
Limestone
Silver/titanium nanoparticles

ABSTRACT

Four biocidal treatments based on nanoparticles were designed and their penetration depths were characterized by laser-induced breakdown spectroscopy (LIBS) technique. This kind of biocidal nanoparticles are being studied to be employed in historic buildings and stone monuments due to their capability to inhibit the growth of biofoulings. The effectiveness of the treatment is related to the penetration depth of the nanoparticles in the limestone pore. For this reason, LIBS depth profiling was used in this work to characterize the diffusion of the nanoparticles in the limestone matrix and to compare the penetration depth of the different treatments. Four different nano-biocides based on silver/titanium dioxide nanoparticles were analysed by LIBS in limestone from Novelda quarry (Alicante, Spain). This limestone has been widely employed in both historical and contemporary buildings in Spain.

The positive detection of the emission line of Ag at 338.289 nm was examined in the depth-related emission spectra as evidence of the presence of the silver nanoparticles and derived nanocomposites in the limestone matrix. The LIBS depth-profiles that were generated, showed a decrease of the Ag net signal with depth due to the diffusion of the nanoparticles in the limestone. Furthermore, the comparison of the in-depth sequences of spectra, and of the Ag depth profiles evidenced penetration differences between the nano-biocides which were explained by differences in the hydrodynamic diameter of the nanoparticles that would affect their diffusion in the limestone pore. The results of this assessment demonstrate the capability and potential of LIBS technique for the in-depth characterization of the nanoparticles and for the comparison of the effectiveness of nanoparticles biocidal treatments based on their penetration in the stone matrix.

Introduction

In the process of historical building restoration, the use of metallic nanomaterials as biocides is one of the most recent advances. Although there are different metallic nanoparticles studied as inhibiting treatments for microorganism and biofouling growth in stone monuments [1–5], it is remarkable the case of silver nanoparticles. The biocidal benefits of silver nanoparticles have been studied in different works [6,7] and the protection that generates this treatment against bacterial development has been successfully used in different applications of diverse fields [8]. Other nanoparticles widely used for cultural heritage are the titanium dioxide (TiO_2) nanoparticles. These nanoparticles have photocatalytic [3,9] and biocide properties [10,11]. The mixture of both nanoparticles in a single nanocomposite enhances the properties of each nanomaterial separately. In this case, photocatalytic capacity of TiO_2 nanoparticles is improved by the biocidal properties of the silver nanoparticles [12,13].

There are important considerations in the application of restoration treatments in stone monuments and buildings to take into account, like the use of innocuous solvents to disperse the nanoparticles [14] or the preservation of the original color of the treated material [15–18]. In addition, the use of nano-biocides requires the evaluation of the restoration effectiveness through the

* Corresponding author.
E-mail address: gines.nicolas@udc.es (G. Nicolás).

https://doi.org/10.1016/j.culher.2022.10.010

measurement of the penetration depth of the nanomaterials. In this sense, the effectiveness of the nano-biocides is related to the capability of the nanoparticle/nanocomposite to penetrate deep in the material for the inhibition of the growth of biodegradation and biocrusts [19]. In some cases, scanning electron microscopy with energy dispersive X-ray spectroscopy (SEM-EDX) has been used to assess the penetration of nanoparticles [20,21], but this technique has some disadvantages such as sample preparation or low sensitivity to detect trace elements [22]. These inconveniences can be eliminated using a spectroscopy technique based on laser ablation (LIBS). This technique employs a pulsed laser beam to irradiate the sample and the analysis of the emission spectrum corresponding to the plasma generated provides the elemental chemical composition of the sample. LIBS is a minimally invasive technique that does not require previous sample preparation, with a higher sensitivity than other techniques such as SEM-EDX and that allows to perform in situ analysis if needed [23,24]. Other advantages of LIBS technique are the possibility to perform the analysis of the sample in the desired location (spatially-resolved analysis) and to achieve depth-profiling without additional equipment. These advantages of LIBS technique have been applied in the Cultural Heritage field [25–34] and to the analysis of nanoparticles in a variety of applications [35–38]. In addition, nanoparticles have been used in LIBS to enhance the signal of the analyte due to a better ablation and excitation efficiency caused by laser electromagnetic field coupling with the induced nanoparticles plasmonic field [39–42]. In previous works [43,44], LIBS technique has been validated for the in-depth analysis of biocides based on nanoparticles by our researcher's groups, but none comparative study of penetration depth of different nano-biocidal treatments by LIBS has been done to date.

Research aim

In this work, LIBS technique is assessed for the analysis and comparison of the penetration depth of different nanocomposites employed as biocides in the restoration of historical buildings and stone monuments. This study was carried out on four treatments based on silver or silver/titanium nanoparticles applied on limestone samples. LIBS in-depth analyses were carried out in these treated samples in order to obtain compositional information from the spectral signal corresponding to different depth levels, characterizing the diffusion of the nanoparticles inside the limestone matrix. From those analyses, in-depth sequences of emission spectra were obtained. The depth-profiles associated to Ag signal were generated and compared for the in-depth characterization of the biocidal nanoparticles, and for the comparison between the different nanocomposites designed as biocidal treatments for stone buildings because their effectiveness is related to their penetration depth into the stone pore.

Materials and methods

Synthesis, characterization and application of treatments

Materials. Silver nitrate ($AgNO_3$), active charcoal (AC) and trisodium citrate from Panreac, sodium borohydride ($NaBH_4$) from Sigma-Aldrich and titanium dioxide (P25) from DEGUSSA were used for the synthesis of the nanocomposites in addition to ultrapure water.

Synthesis. Four biocidal treatments based on silver and titanium dioxide have been prepared and compared. In some cases, trisodium citrate was used as stabilizing agent. Silver/titanium dioxide/active charcoal nanocomposites ($Ag/TiO_2/AC$) were prepared by reduction of silver nitrate with sodium borohydride in aqueous solution [15]. 4 mL of an aqueous solution of $NaBH_4$ (0.01 mmol) were added to 20 mL of an aqueous solution of $AgNO_3$ (0.02 mmol), TiO_2 (10 mg) and active charcoal (1 mg) under magnetic stirring in an ice bath. After 10 min, the resulting suspension was kept in darkness until being applied over stone samples. Silver/titanium dioxide nanocomposites (Ag/TiO_2) were synthesized using the same protocol but without adding active charcoal.

$AgNO_3$ was reduced with $NaBH_4$ in an aqueous solution to synthesize citrate-capped silver nanoparticles (AgCit) and stabilized by trisodium citrate [15]. For that purpose, 1 mL of an aqueous solution of $AgNO_3$ (0.005 mmol) was added to 16 mL of an aqueous solution of trisodium citrate (0.169 mmol) under magnetic stirring in an ice bath. Then, 100 μL of an aqueous solution of $NaBH_4$ (0.01 mmol) were added dropwise. The reaction mixture was stirred for 1 h and 45 min, and the resulting suspension was kept in darkness until being applied over stone samples. Citrate-capped silver /titanium dioxide nanocomposites ($AgCit/TiO_2$) were prepared in the same way but adding 9.6 mg of TiO_2 nanoparticles to the initial 16 mL of aqueous solution containing trisodium citrate.

Stone sample. Limestone slabs (1.5 × 1.5 × 0.5 cm) were employed as stone samples because it is one of the most widely stones used as construction materials since ancient times. The quarry of Novelda (Alicante, Spain) was chosen as the source of slabs because it has been used in both historical and contemporary buildings [45]. This is a biosperite limestone with a low open porosity (5%) (average pore diameter between 0.01 and 0.5 μm) and a high content of quartz and fossil materials [46].

Application of the treatments on limestone slabs. Equal concentration referred to silver nanoparticles (0.015 mg/mL) was employed for each treatment (i.e. 0.015 mg/mL AgCit, 0.145 mg/mL $AgCit/TiO_2$, 0.11 mg/mL $Ag/TiO_2/AC$ or 0.1 mg/mL Ag/TiO_2) by depositing two applications of 200 mL of aqueous suspension of nanocomposites over the surface of each slab. The slabs were dried at room temperature (24 °C ± 2) for three days.

Characterization. The prepared nanocomposites were characterized by Raman spectroscopy (Bruker Senterra confocal Raman microscope, 785 nm laser excitation, DU420A-OE-152 detector), Dynamic Light Scattering (DLS) and UV–Visible (UV–Vis) spectrophotometry. A Zetatrac Analyzer (Microtrac, USA) was used to measure hydrodynamic diameter (HD) by DLS. UV–Vis spectra were registered on an Ocean Optics spectrometer equipped with a HR4000 detector (Dunedin, FL. USA). The color change of the slab surfaces was measured by colorimetry using a colorimeter PCE-CSM 2 (diameter of circular measuring area: 8 mm, daylight illumination: D65). The slab surfaces were analysed before and after application of treatments. Color changes (ΔE^*) were calculated according to the parameters defined by the CIELAB color-system according to Eq. (1).

$$\Delta E^* = \sqrt{\Delta L^{*2} + \Delta a^{*2} + \Delta b^{*2}} \quad \text{(Eq. (1))}$$

where ΔL^*, Δa^* and Δb^* characterize variations of the color values in the brightness (black-white), red-green and yellow-blue axes, respectively.

Penetration depth analyses

The in-depth analysis of the silver-based biocidal treatments was carried out employing a LIBS experimental setup. In particular, a Q-Switched Nd:YAG laser beam (Brilliant, Quantel, 5 ns pulse width, 532 nm, 27 mJ pulse energy) was focused by a plano-convex quartz lens (f = 100 mm) onto the sample surface producing the ablation of the sample and the generation of a plasma. The light emitted by the laser-induced plasma was guided to the entrance slit of an Echelle spectrograph (Mechelle, Andor) by means of a quartz optical fiber. There, the plasma light was dispersed and subsequently it was detected in an ICCD camera (iStar, Andor) in a

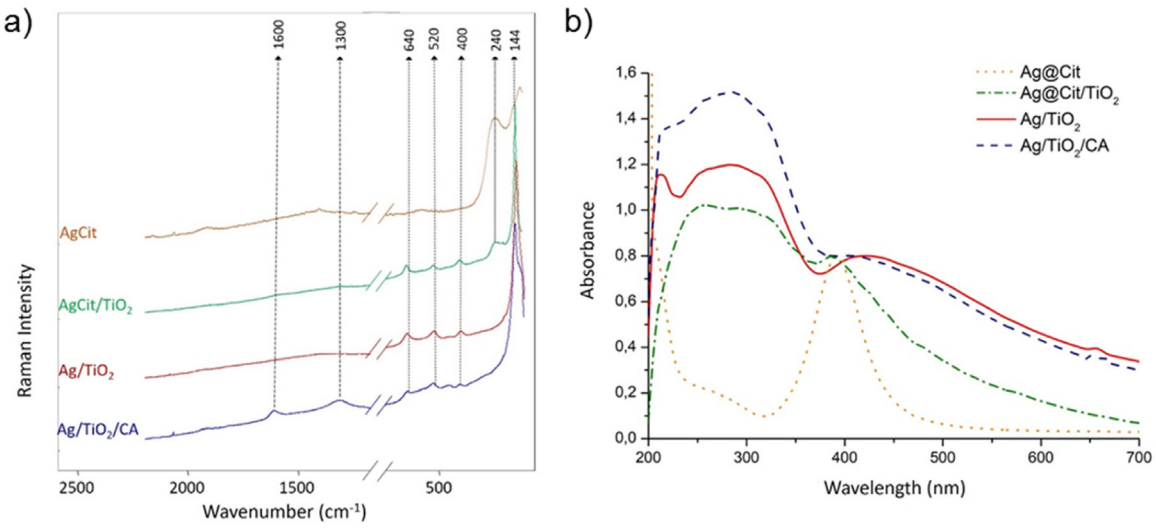

Fig. 1. Raman (a) and UV–Vis (b) spectra of the different nanocomposites.

Table I
Hydrodynamic diameter (HD) of the different types of treatments.

Treatment	Hydrodynamic diameter (nm)
Ag/TiO_2	94±33
Ag/TiO_2/AC	134±18
AgCit	36±8
$AgCit/TiO_2$	72±18

spectral region that covered from 200 to 850 nm. Timing parameters were set at 2.5 μs (delay time) and 10 μs (integration time) for spectral detection. All the LIBS analyses were carried out in air under atmospheric pressure without the need of sample cutting or other type of previous preparation.

It should be noted that the samples were also analyzed by SEM-EDX for comparison, but the sensibility of the technique was not enough to detect the silver at the concentration levels of the nanoparticles in the sample.

Results and discussion

Synthesis, characterization and application of treatments

Four biocidal treatments based on nanoparticles were obtained by reducing silver nitrate with a strong reducing agent, sodium borohydride. Fig. 1a shows the Raman spectra of the four treatments, where spectral differences are evidenced according to their composition. The treatments based on AgCit, $AgCit/TiO_2$ and Ag/TiO_2 have previously been characterized by Raman and UV–Vis [44]. In the case of the treatment based on Ag/TiO_2/AC, it was also possible to detect in the present study the vibrational modes of Ti-O at 144, 400, 520 and 640 cm^{-1} while the presence of AC was indicated by two characteristic peaks at 1300 and 1600 cm^{-1} [47].

The hydrodynamic diameter (HD) of the aqueous dispersions of the different nanocomposites is included in Table I. The lowest HD of the four treatments was obtained for AgCit nanoparticles (36 nm). On the other hand, the treatments without citrate exhibited the highest HD, especially in the case of Ag/ TiO_2/AC (134 nm).

Fig. 2 shows the limestone slabs after deposition of the treatments and the color change (ΔE^*) caused by each treatment. The low porosity (5%) and the size of the stone pores (0.01 and 0.5 μm) made that treatments remained on the stone surfaces and caused their color changes. In the case of cultural heritage, it is a common practice to accept $\Delta E^* < 5$ [48–50]. The treatments based on Ag/TiO_2/AC and AgCit exhibited ΔE^* values nearby to 5, so they could be used for the conservation of monuments. On the other hand, the chromatic changes were more remarkable in the case of the nanocomposites Ag/TiO_2 and $AgCit/TiO_2$ and, consequently, their use should only be recommended in low visual impact areas of monuments, such as cornices or roofs, or when decreasing the concentration of product that is applicated.

Penetration depth analyses

The capability of LIBS technique to detect biocidal treatments based on silver nanocomposites and to analyze their penetration depth into the stone sample has been demonstrated in previous works of our research group [43,44]. However, these studies have been focused on only one biocidal treatment each time: AgCit applied in a quite porous limestone from Utrera quarry [43] and $AgCit/TiO_2$ applied in a low porosity limestone form Novelda quarry. For this reason, the aim of the present study was to continue with the previous ones through the LIBS comparison of the penetration depth of four different biocidal treatments based on silver/titanium nanoparticles in limestone of the same provenance. The main purpose was to know what treatment achieved the highest penetration depth because its penetration is related with its efficiency as biocide. In fact, if a biocide does not have a good penetration depth through the stone pores, the microorganism placed there (endolithic colonization) could recolonize the stone surface (epilithic colonization) in a short time [51]. Because of that, LIBS in-depth compositional analyses were carried out by delivering fifty laser pulses at the same sample position in order to ablate different depth levels and to monitor the spectral signal from the associated laser-induced plasmas. This process was repeated in five distant positions of each sample to obtain representative results. During the analyses, the signal from Ag was monitored as evidence of the presence of the silver nanocomposites. In this sense, the Ag signal detected by LIBS during the depth analysis should totally proceed from the diffused nanoparticles and nanocomposites because the composition of all the biocidal treatments was silver-based, while the limestone matrix from Novelda only could have undetectable traces of silver. In particular, the intensity of Ag (I) 338.289 nm emission line was analyzed in the LIBS spectra of the samples to carry out the penetration depth comparison. It should be noted that other Ag (I) peaks at 328.068, 520.9078 and 546.5497 nm were also detected during the analysis of the samples, as shown in Fig. 3. In this figure, LIBS spec-

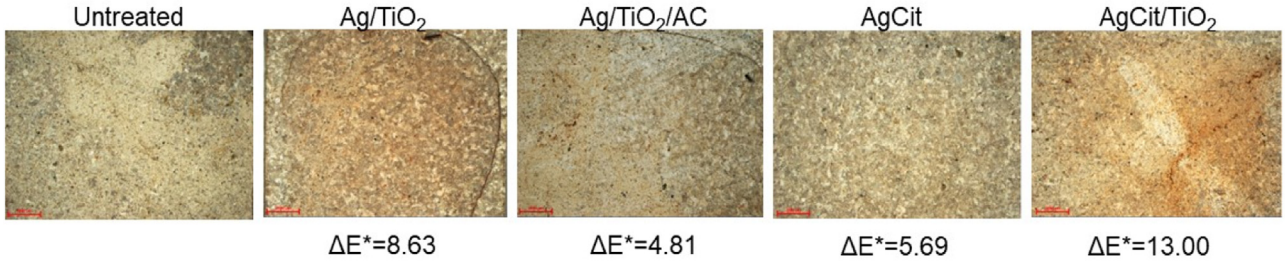

Fig. 2. Photographs of limestone slabs after the application of the treatments based on nanoparticles and nanocomposites and of one slab without any treatment (untreated). Below each photograph appears indicated the color change (ΔE^*) caused by the treatment, according to Eq. (1).

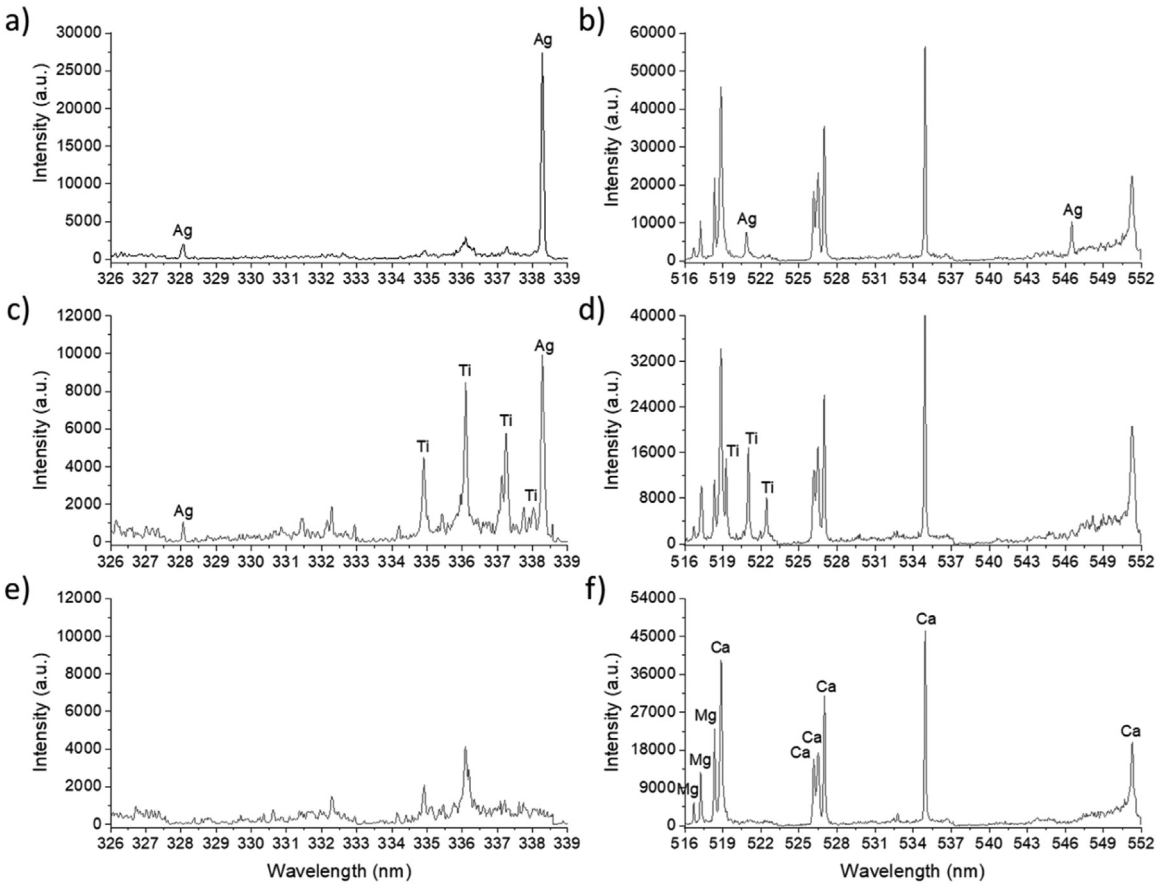

Fig. 3. a) and b) LIBS spectra corresponding to the first in-depth laser pulse of the analysis of the sample treated with AgCit biocide; c) and d) LIBS spectra corresponding to the analysis of the sample treated with AgCit/TiO_2 biocide; e) and f) LIBS spectra corresponding to the analysis of the limestone matrix. Two spectral ranges are shown for each sample.

tra corresponding to the first in-depth pulse of the analysis of the sample treated with AgCit biocide were plotted in two wavelength ranges that include the main emission lines of Ag (Fig. 3a and 3b). As shown, the intensity of the Ag peaks at 328.068, 520.9078 and 546.5497 nm was much weaker than that corresponding to the Ag peak at 338.289 nm and not enough to allow to stablish a reliable trend with depth. In this sense, the Ag peaks around 328, 520 and 546 nm were detected in the first laser shot, corresponding to the analysis of the sample surface where the concentration of the nanoparticles is higher. However, these peaks were hardly distinguished from the background and the peaks of the matrix when analyzing deeper in the samples, due to their lower intensity compared to that of the Ag peak at 338. The same behavior was found in all the samples and is the reason of choosing the Ag emission line around 338 nm to carry out the present study. In the case of the expected more intense emission line of Ag at 328 nm, the authors suggest that the low intensity of this peak observed in the spectra generated from the analysis of the nanoparticles is related to a problem of efficiency at that wavelength of the Echelle spectrometer that is employed in the present study. To discard other possible causes related to the analysis of the nanoparticles or to the limestone matrix, complementary LIBS analyses were performed in several metallic samples of high purity silver, obtaining very similar results: a much lower Ag peak at 328 nm compared to that at 338 nm, which support the author's assumption.

In Fig. 3a and 3b, the rest of peaks in the spectra different than Ag were attributed to the matrix. LIBS spectra corresponding to the analysis of the sample treated with AgCit/TiO_2 biocide are plotted in Fig. 3c and 3d, where several lines of Ti were detected: Ti (II) 334.904–334.941, 336.121, 337.28 and 338.028 nm and Ti (I) 519.298–519.404, 521.0384 and 522.269–522.495 nm. It should be noted that, although close, the Ag peak at 520.9078 nm and the

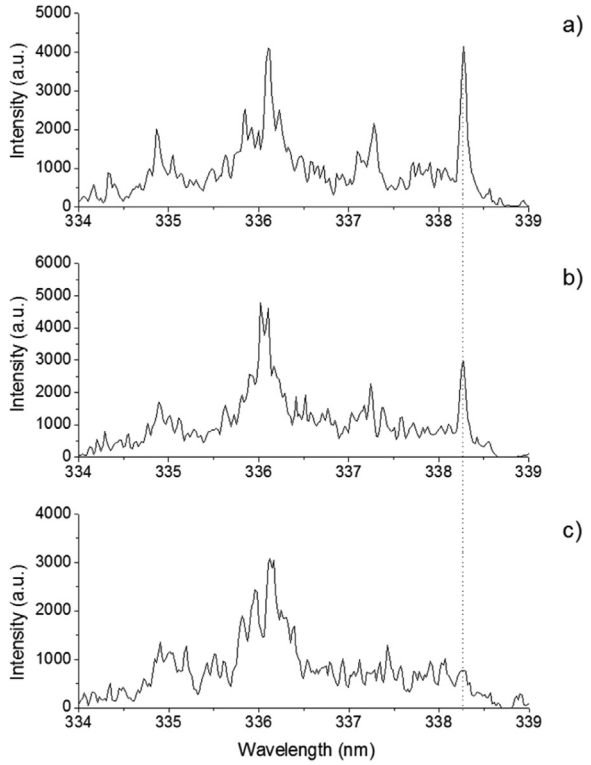

Fig. 4. LIBS spectra corresponding to the in-depth laser pulse 31 (estimated depth of 186 µm) from limestone samples treated with a) AgCit/TiO_2, b) Ag/TiO_2 and c) Ag/TiO_2/AC. The peak identified as Ag has been indicated in the spectra by a dotted line.

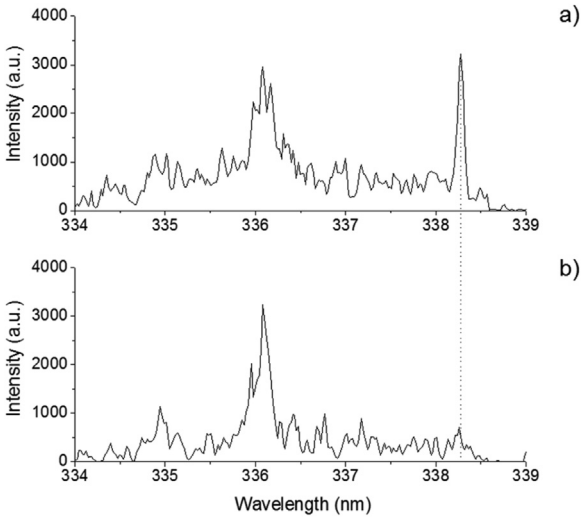

Fig. 5. LIBS spectra corresponding to the in-depth laser pulse 43 (estimated depth of 258 µm) from limestone samples treated with a) AgCit and b) AgCit/TiO_2. The peak identified as Ag has been indicated in the spectra by a dotted line.

Ti peak at 521.0384 nm were enough resolved to be differentiated. In addition, as commented before, the Ag peaks at 520.9078 and at 546.5497 nm were only detected in the first laser pulse but not deeper inside, in contrast to that of Ti at 521.0384 nm. This fact is evidenced in the spectrum of Fig. 3d corresponding to the second in-depth pulse. Spectra of the limestone matrix were plotted in Fig. 3e and 3f in the same ranges than the lines of interest, for comparison. In Fig. 3e, the peaks from the limestone matrix were not enough intense and well-resolved to allow an exact identification. In contrast, in Fig. 3f, the main peaks corresponding to the limestone matrix have been labeled: Mg (I) 516.733, Mg (I) 517.268, Mg (I) 518.361, Ca (I) 518.885, Ca (I) 526.171, Ca (I) 526.224–526.556, Ca (I) 527.027, Ca (I) 534.947 and Ca (I) 551.298 nm.

The penetration depth study was carried out by analyzing the Ag intensity at 338.289 nm in the depth-related spectra to compare the depth reached by the different nano-biocides. This emission line was selected due to its intensity, as shown previously, and because Ag was present in all the treatments under study, in contrast to Ti. Figs. 4 and 5 show several spectra corresponding to the same in-depth laser pulse for samples with different treatments around the wavelength of interest. In this sense, the emission spectra of Fig. 4 correspond to pulse 31 and those of Fig. 5 to pulse 43. In order to compare the penetration of the nanoparticles, it was necessary to convert the number of laser pulses into depth by calculating an approximate ablation rate [43], that is, the depth eroded in each laser pulse. For that purpose, a varied number of depth laser pulses were delivered in the treated samples to generate different craters which depth was measured by optical microscopy. Afterwards, the measured depth of the craters was divided by the corresponding number of delivered laser pulses to calculate an average ablation-rate of 6 µm/pulse. It should be noted that no significant differences were found in the ablation rate calculated for the samples treated with the four nano-biocides. Using an average ablation-rate value of 6 µm/pulse, LIBS spectra of Fig. 4 were related to a depth of 186 µm and those of Fig. 5 to a depth of 258 µm.

Fig. 4 shows the spectra acquired from the in-depth analysis of three of the treated samples, AgCit/TiO_2, Ag/TiO_2 and Ag/TiO_2/AC, at a depth closer to the sample surface, at 186 µm. The comparison of these spectra revealed that the Ag peak was clearly visible in the spectrum corresponding to the AgCit/TiO_2 treatment (Fig. 4a) at that depth level. In the case of naked-silver nanocomposites, while in the spectrum of Ag/TiO_2 sample (Fig. 4b) could be still distinguished the Ag peak at 338.289 nm from the noise, in the spectrum from the Ag/TiO_2/AC sample (Fig. 4c) was not detected. This result indicates that the Ag/TiO_2/AC treatment did not diffuse so deep in the limestone in contrast to AgCit/TiO_2 and Ag/TiO_2 nanocomposites, and therefore that the AgCit/TiO_2 treatment exhibits a higher penetration in the matrix, followed by Ag/TiO_2, compared to that of Ag/TiO_2/AC treatment.

Fig. 5 exhibits the LIBS spectra corresponding to the analysis of the samples treated with citrate-capped silver nanocomposites, at a depth of 258 µm. As shown, the Ag peak was clearly visible in the spectrum corresponding to the AgCit nanoparticles (Fig. 5a) at that depth level, however, the Ag peak at 338.289 nm was not detected in the spectrum from the AgCit/TiO_2 sample (Fig. 5b). This result indicates that the AgCit/TiO_2 nano-biocide did not reach that depth level in the limestone in contrast to AgCit nanoparticles, and therefore that the AgCit treatment exhibits a higher penetration in the matrix compared to that of AgCit/TiO_2.

Following with the penetration depth analysis, and in order to confirm the conclusions attained from the comparison of the in-depth spectra corresponding to the different biocidal treatments, LIBS depth profiles were generated from the previously acquired data. For this purpose, the Ag net intensity of each spectrum was plotted versus the corresponding number of laser pulses of the depth sequence. The Ag net intensity was calculated from the signal of the Ag (I) 338.289 nm emission line after subtraction of the continuum background measured in the spectral range 336.35–336.82 nm. This spectral window was selected because it is close to the Ag peak and it was free of peaks.

Some LIBS depth profiles generated in such a way and corresponding to the analysis of the four treated samples are plotted in Fig. 6. As shown, all the profiles exhibited a decay trend of Ag intensity with the number of in-depth laser pulses. This de-

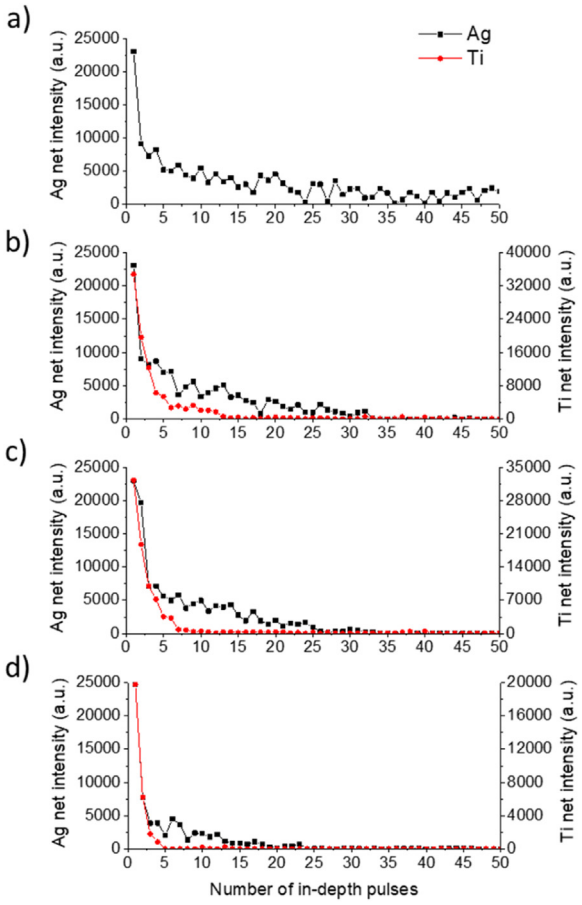

Fig. 6. LIBS depth profiles of Ag (square) and Ti (circle) net intensity from limestone samples treated with a) AgCit b) AgCit/TiO_2, c) Ag/TiO_2 and d) Ag/TiO_2/AC. The Ti depth profile of the sample treated with AgCit has not been plotted because the Ti is not present in that treatment.

crease of the signal was an expected result because it agrees with the diffusion of the silver-based nanoparticles and nanocomposites inside the limestone matrix. The small intensity fluctuations observed in the depth profiles of Fig. 6 was attributed to the effect of the porosity and heterogeneity of the stone in the diffusion of the nano-biocides. As shown in the depth profile of Fig. 6a, corresponding to the treatment with AgCit nanoparticles, the Ag signal was low after 35 in-depth laser pulses but it can be still detected, in contrast to the depth profiles of the other samples. This result indicates a higher penetration of the AgCit nanoparticles compared with the other treatments, which can be explained by the lower hydrodynamic diameter of these silver nanoparticles. In the depth profile of the AgCit/TiO_2 sample (Fig. 6b), the Ag net intensity was negligible after 33 pulses, while in the profiles of the Ag/TiO_2 sample (Fig. 6c) the signal was very low after 26 pulses and it completely disappeared after 33 pulses. In the Ag profile of Fig. 6d, corresponding to the sample with Ag/TiO_2/AC, no Ag signal was observed after about 24 pulses. These results indicate that AgCit nanoparticles diffuse deeper inside the stone matrix than the other treatments, followed by its TiO_2-derived nanocomposite. Ag/TiO_2/AC nanocomposite seems to be the lowest efficient nanobiocide in terms of penetration depth.

With the aim of comparison, the LIBS depth profiles corresponding to Ti net intensity were also included in Fig. 6 for the three biocidal treatments which contains that element. The Ti net intensity was calculated from the signal of the Ti (I) 521.0384 nm emission line after subtraction of the continuum background measured in the spectral range 521.47–521.79 nm. It should be noted that, although the Ti profiles of Fig. 6 correspond to the net signal of Ti (I) 521.0384 nm emission line, other Ti emission lines (Ti II 368.52, Ti II 337.28, and Ti I 451.803 nm) were tested with very similar results to those plotted. As shown in Fig. 6, all the Ti profiles exhibited a decay trend of signal with the number of in-depth laser pulses, as the presence of nanocomposites decreases with depth, corroborating the results obtained for Ag. In Fig. 6, although the trend of Ti profiles is the same than that of Ag profiles, however, the Ag signals take more pulses to disappear than the Ti signals. This effect was also observed for the AgCit/TiO_2 treatment in a previous research [44] and the cause is still under study, but the possibility of the presence of different types of nanoparticles with different penetrations after the treatment is being considered. Anyway, as Ag is the element common to all the treatments under comparison, the penetration study has centered on it.

In order to carry out a quantitative comparison of the penetration depth of the different treatments, the laser pulse from which the Ag signal disappeared in the LIBS in-depth analyses was converted into depth with the use of the average ablation rate previously calculated. That resulting depth was representative of the penetration of the corresponding treatment because it indicated the depth from which the signal from the nano-biocide was not detected. The penetration values estimated in such a way have been included in Table II for five different positions analyzed in each treated sample under the same experimental conditions. As shown in the table, the calculated penetration range of the biocidal treatments in the limestone matrix was 246–276 μm, 156–228 μm, 156–192 μm and 138–168 μm for AgCit, AgCit/TiO_2, Ag/TiO_2 and Ag/TiO_2/AC treatments, respectively. It should be noted that, although an average value of penetration have been calculated, instead of that, the authors prefer to provide penetration ranges to take into account variations in the diffusion of the treatments due to the porosity and heterogeneity of the limestone pore system. From the values of Table II, the lowest penetration can be assigned to Ag/TiO_2/AC nanocomposites, followed by Ag/TiO_2 and AgCit/TiO_2, while the highest penetration corresponds to the AgCit nanoparticles. These results are in agreement with the hydrodynamic diameter of the different types of treatments (see Table I): Ag/TiO_2/AC> Ag/TiO_2> AgCit/TiO_2> AgCit: the bigger the hydrodynamic diameter, the lower the penetration depth. Therefore, the AgCit nanoparticles seems to be the most effective biocidal treatment for limestones in terms of depth penetration. To corroborate the results of this comparison, the penetration depth of three of the biocides was calculated from the Ti analysis, resulting in penetration ranges of 66–72 μm, 36–42 μm, and 18–30 μm for AgCit/TiO_2, Ag/TiO_2 and Ag/TiO_2/AC, respectively. Although the values are different than those obtained from the analysis of Ag, due to the earlier disappearance of Ti signal, the order of the biocidal treatments in terms of penetration depth is the same than with Ag, confirming the results.

It should be noted that, despite its interest, the penetration depth of biocidal treatments based on nanoparticles is not usually measured due to the difficulty of conventional analytical techniques to detect, with spatial resolution, the nanoparticles at the low concentration levels employed. In this sense, in a previous work [43], Ag was not detected in one of the treatments used in this study, AgCit, by SEM-EDX, even when using higher concentrations. In this work there were fresh attempts in the four treatments with no success. As a consequence, the penetration data presented in this work could not be validated by another analytical technique nor the possibility of the presence of different types of nanoparticles with different penetrations. This fact, although is an inconvenient, demonstrates the usefulness of LIBS technique in the restoration field related to nano-biocidal protection, and its potential for the characterization and comparison of nano-biocidal treat-

Table II
Penetration values (μm) of the different types of treatments in Novelda limestone, estimated from LIBS in-depth analysis of Ag.

Number of analysis	AgCit penetration (μm)	AgCit/TiO_2 penetration (μm)	Ag/TiO_2 penetration (μm)	Ag/TiO_2/AC penetration (μm)
1	246	156	192	168
2	276	204	192	144
3	270	168	156	156
4	276	204	168	138
5	270	228	180	168
Average	268±12	192±29	178±16	154±14

ments effectiveness from the analysis of the penetration depth of the nanoparticles.

Conclusions

The effectiveness of the nano-biocides employed for the protection of historic buildings and stone monuments is related to the capability of the treatments to reach the same depth that the microorganism colonies to inhibit them. For this reason, it is necessary to measure the penetration depth of the nano-biocides in order to characterize their effectiveness. In this study, LIBS technique has been successfully used for the analysis and comparison of the penetration depth of four biocidal treatments (silver nanoparticles and silver/titanium dioxide nanocomposites: AgCit, AgCit/TiO_2, Ag/TiO_2, Ag/TiO_2/AC) in limestone samples. For this purpose, several in-depth analyses were carried out by LIBS in different positions of each treated sample in order to obtain depth-related spectra. The presence of the emission line of Ag at 338.289 nm was studied in those emission spectra as evidence of the presence of the silver nanoparticles and derived nanocomposites in the Novelda limestone. Depth profiles were generated by plotting the evolution of the net Ag intensity with the increase of the number of in-depth laser pulses. For comparison, complementary depth profiles of Ti net signal were also generated. Both, the in-depth spectra sequences and the depth profiles evidenced the decrease of Ag and Ti signal with depth, in agreement with the diffusion of the treatments in the limestone, and showed penetration differences between the nano-biocides. In this sense, after the conversion of laser pulses into depth, the calculated penetration depth of the biocidal treatments decreased in the following order: AgCit> AgCit/TiO_2> Ag/TiO_2> Ag/TiO_2/AC. This result was explained by the increasing hydrodynamic diameter that complicated the diffusion of the nanoparticles in the stone matrix, especially in the case of a low porosity and low medium average pore size limestone as the limestone from Novelda.

In conclusion, the capability of LIBS technique has been demonstrated in this work for the characterization and comparison of nano-biocidal treatments effectiveness from the analysis of the penetration depth of the nanocomposites. Considering the difficulty of other analytical techniques to provide that information, these results evidence the potential of LIBS technique as a characterization tool in the restoration field related to nano-biocidal protective treatments.

Acknowledgements

This study has been partially supported by the projects: Art-Risk (RETOS project of Ministerio de Economía y Competitividad and Fondo Europeo de Desarrollo Regional (FEDER), code: BIA2015–64878-R (MINECO/FEDER, UE)), CTQ2013–48396-P of Fondo Europeo de Desarrollo Regional (FEDER-Unión Europea) and Ministerio Economía y Competitividad and the research teams P10-FQM-6615, TEP-199 and FQM-319 from Junta de Andalucía. J. Becerra is grateful to the Ministerio de Educación, Cultura y Deporte for his pre-doctoral fellowship (FPU14/05348). The authors are also grateful to Universidade da Coruña/CISUG for the funding of open access charge.

References

[1] A.M.M. Essa, M.K. Khallaf, Biological nanosilver particles for the protection of archaeological stones against microbial colonization, Int. Biodeterior. Biodegrad. 94 (2014) 31–37, doi:10.1016/j.ibiod.2014.06.015.
[2] R. Carrillo-González, M.A. Martínez-Gómez, M. del C.A. González-Chávez, J.C. Mendoza Hernández, Inhibition of microorganisms involved in deterioration of an archaeological site by silver nanoparticles produced by a green synthesis method, Sci. Total Environ. 565 (2015) 872–881, doi:10.1016/j.scitotenv.2016.02.110.
[3] P. Munafò, G.B. Goffredo, E. Quagliarini, TiO2-based nanocoatings for preserving architectural stone surfaces: an overview, Constr. Build. Mater. 84 (2015) 201–218, doi:10.1016/j.conbuildmat.2015.02.083.
[4] L. Graziani, E. Quagliarini, A. Osimani, L. Aquilanti, F. Clementi, C. Yéprémian, V. Lariccia, S. Amoroso, M. D'Orazio, Evaluation of inhibitory effect of TiO2 nanocoatings against microalgal growth on clay brick façades under weak UV exposure conditions, Build. Environ. 64 (2013) 38–45, doi:10.1016/j.buildenv.2013.03.003.
[5] I.D. Van der Werf, N. Ditaranto, R.A. Picca, M.C. Sportelli, L. Sabbatini, Development of a novel conservation treatment of stone monuments with bioactive nanocomposites, Herit. Sci. 3 (2015) 29, doi:10.1186/s40494-015-0060-3.
[6] M. Rai, A. Yadav, A. Gade, Silver nanoparticles as a new generation of antimicrobials, Biotechnol. Adv. 27 (2009) 76–83, doi:10.1016/j.biotechadv.2008.09.002.
[7] J.S. Kim, E. Kuk, K.N. Yu, J.H. Kim, S.J. Park, H.J. Lee, S.H. Kim, Y.K. Park, Y.H. Park, C.Y. Hwang, Y.K. Kim, Y.S. Lee, D.H. Jeong, M.H. Cho, Antimicrobial effects of silver nanoparticles, Nanomedicine Nanotechnology, Biol. Med. 3 (2007) 95–101, doi:10.1016/j.nano.2006.12.001.
[8] B. Gutarowska, J. Skora, K. Zduniak, D. Rembisz, Analysis of the sensitivity of microorganisms contaminating museums and archives to silver nanoparticles, Int. Biodeterior. Biodegrad. 68 (2012) 7–17, doi:10.1016/j.ibiod.2011.12.002.
[9] E. Quagliarini, F. Bondioli, G.B. Goffredo, C. Cordoni, P. Munafò, Self-cleaning and de-polluting stone surfaces: tiO2 nanoparticles for limestone, Constr. Build. Mater. 37 (2012) 51–57, doi:10.1016/j.conbuildmat.2012.07.006.
[10] M.F. La Russa, S.A. Ruffolo, N. Rovella, C.M. Belfiore, A.M. Palermo, M.T. Guzzi, G.M. Crisci, Multifunctional TiO2 coatings for Cultural Heritage, Prog. Org. Coatings. 74 (2012) 186–191, doi:10.1016/j.porgcoat.2011.12.008.
[11] H.A. Foster, I.B. Ditta, S. Varghese, A. Steele, Photocatalytic disinfection using titanium dioxide: spectrum and mechanism of antimicrobial activity, Appl. Microbiol. Biotechnol. 90 (2011) 1847–1868, doi:10.1007/s00253-011-3213-7.
[12] I. Yaşa, N. Lkhagvajav, M. Koizhaiganova, E. Çelik, Ö. Sari, Assessment of antimicrobial activity of nanosized Ag doped TiO2 colloids, World J. Microbiol. Biotechnol. 28 (2012) 2531–2539, doi:10.1007/s11274-012-1061-y.
[13] M. Lungu, Ş. Gavriliu, E. Enescu, I. Ion, A. Brătulescu, G. Mihăescu, L. Măruţescu, M.C. Chifiriuc, Silver–titanium dioxide nanocomposites as effective antimicrobial and antibiofilm agents, J. Nanoparticle Res. 16 (2014) 2203, doi:10.1007/s11051-013-2203-3.
[14] F. Bellissima, M. Bonini, R. Giorgi, P. Baglioni, G. Barresi, G. Mastromei, B. Perito, Antibacterial activity of silver nanoparticles grafted on stone surface, Environ. Sci. Pollut. Res. 21 (2014) 13278–13286, doi:10.1007/s11356-013-2215-7.
[15] J. Becerra, A.P. Zaderenko, M.J. Sayagués, R. Ortiz, P. Ortiz, Synergy achieved in silver-TiO2 nanocomposites for the inhibition of biofouling on limestone, Build. Environ. 141 (2018) 80–90, doi:10.1016/j.buildenv.2018.05.020.
[16] J. Becerra, A.P. Zaderenko, P. Ortiz, Silver/dioxide titanium nanocomposites as biocidal treatments on limestones, Ge-Conservación 11 (2017) 141–148.
[17] M.F. La Russa, A. Macchia, S.A. Ruffolo, F. De Leo, M. Barberio, P. Barone, G.M. Crisci, C. Urzì, Testing the antibacterial activity of doped TiO2 for preventing biodeterioration of cultural heritage building materials, Int. Biodeterior. Biodegrad. 96 (2014) 87–96, doi:10.1016/j.ibiod.2014.10.002.
[18] E. Quagliarini, F. Bondioli, G.B. Goffredo, A. Licciulli, P. Munafò, Self-cleaning materials on Architectural Heritage: compatibility of photo-induced hydrophilicity of TiO2 coatings on stone surfaces, J. Cult. Herit. 14 (2013) 1–7, doi:10.1016/j.culher.2012.02.006.
[19] M.M. Mansour, Proactive investigation using bioagents and fungicide for preservation of Egyptian stone sarcophagus, J. Appl. Sci. Res. 9 (2013) 1917–1930.
[20] G. Borsoi, R. Van Hees, B. Lubelli, R. Veiga, A.Santos Silva, Nanolime deposition in Maastricht limestone : back-migration or accumulation at the absorp-

tion surface? in: EMABM 2015 Proc. 15th Euroseminar Microsc. Appl. to Build. Mater. Delft, Netherlands, University of Technology, Delft, 2015, pp. 77–86. 17-19 June 2015, Delft.
[21] F. Gherardi, A. Colombo, M. D'Arienzo, B. Di Credico, S. Goidanich, F. Morazzoni, R. Simonutti, L. Toniolo, Efficient self-cleaning treatments for built heritage based on highly photo-active and well-dispersible TiO2 nanocrystals, Microchem. J. 126 (2016) 54–62, doi:10.1016/j.microc.2015.11.043.
[22] B. Kearton, Y. Mattley, Laser-induced breakdown spectroscopy: sparking new applications, Nat. Photonics. 2 (2008) 537–540, doi:10.1038/nphoton.2008.173.
[23] F.C. De Lucia, A.W. Miziolek, K.L. Mcnesby, R.A. Walters, P.D. French, Laser-induced breakdown spectroscopy (LIBS) – an emerging field-portable sensor technology for real-time, in-situ geochemical and environmental analysis, Geochemistry Explor. Environ. Anal. 5 (2005) 21–28.
[24] D. Anglos, V. Detalle, Cultural Heritage Application of LIBS, in: Laser-Induced Break, Spectrosc, 2014, pp. 531–554, doi:10.1007/978-3-642-45085-3.
[25] F. Colao, R. Fantoni, P. Ortiz, M.A.A. Vazquez, J.M.M. Martin, R. Ortiz, N. Idris, Quarry identification of historical building materials by means of laser induced breakdown spectroscopy, X-ray fluorescence and chemometric analysis, Spectrochim. Acta Part B At. Spectrosc. 65 (2010) 688–694, doi:10.1016/j.sab.2010.05.005.
[26] S. Awasthi, R. Kumar, G.K. Rai, A.K. Rai, Study of archaeological coins of different dynasties using libs coupled with multivariate analysis, Opt. Lasers Eng. 79 (2016) 29–38, doi:10.1016/j.optlaseng.2015.11.005.
[27] L. Caneve, A. Diamanti, F. Grimaldi, G. Palleschi, V. Spizzichino, F. Valentini, Analysis of fresco by laser induced breakdown spectroscopy, Spectrochim. Acta - Part B At. Spectrosc. 65 (2010) 702–706, doi:10.1016/j.sab.2010.05.003.
[28] S. Guirado, F.J. Fortes, V. Lazic, J.J. Laserna, Chemical analysis of archeological materials in submarine environments using laser-induced breakdown spectroscopy. On-site trials in the Mediterranean Sea, Spectrochim. Acta - Part B At. Spectrosc. 74–75 (2012) 137–143, doi:10.1016/j.sab.2012.06.032.
[29] S. Mahmood, S.A. Abbasi, S. Jabeen, M.A. Baig, Laser-induced breakdown spectroscopic studies of marbles, J. Quant. Spectrosc. Radiat. Transf. 111 (2010) 689–695, doi:10.1016/j.jqsrt.2009.11.012.
[30] P. Ortiz, V. Antúnez, R. Ortiz, J.M. Martín, M.A. Gómez, A.R. Hortal, B. Martínez-Haya, Comparative study of pulsed laser cleaning applied to weathered marble surfaces, Appl. Surf. Sci. 283 (2013) 193–201, doi:10.1016/j.apsusc.2013.06.081.
[31] P. Ortiz, V. Antunez, R. Ortiz, J.M. Ramírez, M.A. Gómez, M. Bethencourt, I. López, V. Piñón, M.P. Mateo, G. Nicolás, IV Congreso Latinoamericano de Conservación y Restauración de Metal, in: Grupo Español de Conservación (Ed.), IV Congr. Latinoam. Conserv. y Restauración Met., Madrid, 2013: pp. 41–48.
[32] D. Syvilay, V. Detalle, N. Wilkie-Chancellier, A. Texier, L. Martinez, S. Serfaty, Novel approach of signal normalization for depth profile of cultural heritage materials, Spectrochim. Acta - Part B At. Spectrosc. 127 (2017) 28–33, doi:10.1016/j.sab.2016.11.001.
[33] P. Siozos, A. Philippidis, D. Anglos, Portable laser-induced breakdown spectroscopy/diffuse reflectance hybrid spectrometer for analysis of inorganic pigments, Spectrochim. Acta - Part B At. Spectrosc. 137 (2017) 93–100, doi:10.1016/j.sab.2017.09.005.
[34] A. Brysbaert, P. Siozos, M. Vetters, A. Philippidis, D. Anglos, Materials analyses of pyrotechnological objects from LBA Tiryns, Greece, by means of Laser-Induced Breakdown Spectroscopy (LIBS): results and a critical assessment of the method, J. Archaelog. Sci. 83 (2017) 49–61, doi:10.1016/j.jas.2017.06.007.
[35] L. Krajcarová, K. Novotný, M. Kummerová, J. Dubová, V. Gloser, J. Kaiser, Mapping of the spatial distribution of silver nanoparticles in root tissues of Vicia faba by laser-induced breakdown spectroscopy (LIBS), Talanta 173 (2017) 28–35, doi:10.1016/j.talanta.2017.05.055.
[36] O. Picard, J. Sirven, J.-.B. Sublemontier, On-line Monitoring of Nanoparticle Synthesis by Laser-Induced Breakdown Spectroscopy in Vacuum, MRS Adv 2 (2017) 1487–1491, doi:10.1557/adv.2016.633.
[37] T. Amodeo, C. Dutouquet, F. Tenegal, B. Guizard, H. Maskrot, O.Le Bihan, E. Fréjafon, On-line monitoring of composite nanoparticles synthesized in a pre-industrial laser pyrolysis reactor using Laser-Induced Breakdown Spectroscopy, Spectrochim. Acta - Part B At. Spectrosc. 63 (2008) 1183–1190, doi:10.1016/j.sab.2008.09.005.
[38] J. Menneveux, F. Wang, S. Lu, X. Bai, V. Motto-Ros, N. Gilon, Y. Chen, J. Yu, Direct determination of Ti content in sunscreens with laser-induced breakdown spectroscopy: line selection method for high TiO2 nanoparticle concentration, Spectrochim. Acta - Part B At. Spectrosc. 109 (2015) 9–15, doi:10.1016/j.sab.2015.04.010.
[39] A. De Giacomo, M. Dell'Aglio, R. Gaudiuso, C. Koral, G. Valenza, Perspective on the use of nanoparticles to improve LIBS analytical performance: nanoparticle enhanced laser induced breakdown spectroscopy (NELIBS), J. Anal. At. Spectrom. 31 (2016) 1566–1573, doi:10.1039/C6JA00189K.
[40] A. De Giacomo, R. Gaudiuso, C. Koral, M. Dell'Aglio, O. De Pascale, Nanoparticle-enhanced laser-induced breakdown spectroscopy of metallic samples, Anal. Chem. 85 (2013) 10180–10187, doi:10.1021/ac4016165.
[41] M. Dell'Aglio, R. Alrifai, A. De Giacomo, Nanoparticle Enhanced Laser Induced Breakdown Spectroscopy (NELIBS), a first review, Spectrochim. Acta - Part B At. Spectrosc. 148 (2018) 105–112, doi:10.1016/j.sab.2018.06.008.
[42] C. Koral, M. Dell'Aglio, R. Gaudiuso, R. Alrifai, M. Torelli, A. De Giacomo, Nanoparticle-Enhanced Laser Induced Breakdown Spectroscopy for the noninvasive analysis of transparent samples and gemstones, Talanta 182 (2018) 253–258, doi:10.1016/j.talanta.2018.02.001.
[43] M. Mateo, J. Becerra, A.P. Zaderenko, P. Ortiz, G. Nicolás, Laser-induced breakdown spectroscopy applied to the evaluation of penetration depth of bactericidal treatments based on silver nanoparticles in limestones, Spectrochim. Acta Part B At. Spectrosc. 152 (2019) 44–51, doi:10.1016/j.sab.2018.11.010.
[44] J. Becerra, M. Mateo, P. Ortiz, G. Nicolás, A.P. Zaderenko, Evaluation of the applicability of nano-biocide treatments on limestones used in cultural heritage, J. Cult. Herit. In press (2019), doi:10.1016/j.culher.2019.02.010.
[45] R. Fort, A. Bernabéu, M.A. García del Cura, M.C. López de Azcona, S. Ordóñez, F. Mingarro, Novelda Stone: widely used within the Spanish architectural heritage, Mater. Construcción. 52 (2002) 19–32, doi:10.3989/mc.2002.v52.i266.332.
[46] M.A. Guerrero, Diagnóstico Del Estado De Alteración De La Piedra Del Palacio Consistorial De Sevilla. Causas y mecanismos, Universidad de Sevilla (Spain), 1990.
[47] Y. Xie, Y. Meng, SERS performance of graphene oxide decorated silver nanoparticle/titania nanotube array, RSC Adv 4 (2014) 41734–41743, doi:10.1039/C4RA07865A.
[48] P. Sanmartín, F. Villa, A. Polo, B. Silva, B. Prieto, F. Cappitelli, Rapid evaluation of three biocide treatments against the cyanobacterium Nostoc sp. PCC 9104 by color changes, Ann. Microbiol. 65 (2015) 1153–1158, doi:10.1007/s13213-014-0882-3.
[49] L. Pinho, M. Rojas, M.J. Mosquera, Ag–SiO2–TiO2 nanocomposite coatings with enhanced photoactivity for self-cleaning application on building materials, Appl. Catal. B Environ. 178 (2015) 144–154, doi:10.1016/j.apcatb.2014.10.002.
[50] L. Graziani, E. Quagliarini, M. D'Orazio, The role of roughness and porosity on the self-cleaning and anti-biofouling efficiency of TiO2-Cu and TiO2-Ag nanocoatings applied on fired bricks, Constr. Build. Mater 129 (2016) 116–124, doi:10.1016/j.conbuildmat.2016.10.111.
[51] A.Z. Miller, P. Sanmartín, L. Pereira-Pardo, A. Dionísio, C. Saiz-Jimenez, M.F. Macedo, B. Prieto, Bioreceptivity of building stones: a review, Sci. Total Environ. 426 (2012) 1–12, doi:10.1016/j.scitotenv.2012.03.026.